Earth Surf. Dynam. Discuss., https://doi.org/10.5194/esurf-2017-60
Manuscript under review for journal Earth Surf. Dynam.
Discussion started: 1 November 2017

Earth Surface Dynamics Discussions

Unsupervised detection of salt marsh platforms: a topographic method

Guillaume C. H. Goodwin[1], Simon M. Mudd[1], and Fiona J. Clubb[1,2]

[1]School of Geosciences, University of Edinburgh
[2]Department of Earth Sciences and St. Anthony Falls Laboratory, University of Minnesota, Minneapolis, MN, USA

Correspondence to: Guillaume C. H. Goodwin (g.c.h.goodwin@sms.ed.ac.uk)

Abstract.

Salt marshes filter pollutants, protect coastlines against storm surges, and sequester carbon, yet are under threat from sea level rise and anthropogenic modification. The productivity and even survival of salt marsh vegetation depends on the topographic evolution of marsh platforms. Quantifying marsh platform topography is vital for improving the management of these valuable landscapes. Determining platform boundaries currently relies on supervised classification methods requiring near-infrared data to detect vegetation, or demands labor-intensive field surveys and digitization. We propose a novel, unsupervised method to reproducibly isolate saltmarsh scarps and platforms from a DEM, referred to as Topographic Identification of Platforms (TIP). Field observations and numerical models show that saltmarshes mature into sub-horizontal platforms delineated by sub-vertical scarps: based on this premise, we identify scarps as lines of local maxima on a slope raster, then fill landmasses from the scarps upward, thus isolating mature marsh platforms. We test the TIP method using lidar-derived DEMs from six saltmarshes in England with varying tidal ranges and geometries, for which topographic platforms were manually distinguished from tidal flats. Agreement between manual and unsupervised classification exceeds 94% for DEM resolutions of 1 m, with all but one sites maintaining an accuracy superior to 90% for resolutions up to 3 m. For resolutions of 1 m, platforms detected with the TIP method are comparable in surface area to digitized platforms, and have similar elevation distributions. We also find that our method allows the accurate detection of local bloc failures as small as 3 times the DEM resolution. Detailed inspection reveals that although tidal creeks were digitized as part of the marsh platform, unsupervised classification categorizes them as part of the tidal flat, causing an increase in false negatives and overall platform perimeter. This suggests our method would have increased accuracy if used in combination with existing creek detection algorithms. Fallen blocs and high tidal flat portions, associated with potential pioneer zones, may also be areas of discordance between our method and supervised mapping. Although pioneer zones prove difficult to classify using a topographic method, it also suggests that these transition areas should be considered when analysing erosion and accretion processes, particularly in the case of incipient marsh platforms. Ultimately, we have shown that unsupervised classification of marsh platforms from high-resolution topography is possible and sufficient to monitor and analyze topographic evolution.

Earth Surf. Dynam. Discuss., https://doi.org/10.5194/esurf-2017-60
Manuscript under review for journal Earth Surf. Dynam.
Discussion started: 1 November 2017

1 Introduction

Salt marshes are highly dynamic ecosystems, sequestrating on average 210 g CO_2 m^{-2} yr^{-1} through plant growth and decay (Chmura et al., 2003) and capturing additional inorganic sediment when they are submerged (Nardin and Edmonds, 2014). This productivity has allowed salt marshes to match historic sea level rise (Kirwan and Temmerman, 2009) and laterally expand when sediment inputs were sufficient (Kirwan et al., 2011). It also places them among the most valuable ecosystems in the world (Costanza et al., 1997), and they provide diverse ecosystem services such as flood attenuation (Möller and Spencer, 2002; Shepard et al., 2011), blue carbon sequestration (Chmura et al., 2003; Coverdale et al., 2014), and contaminant capture (Nelson and Zavaleta, 2012). Their economic value combined with their alarming retreat (Day et al., 2000; Duarte et al., 2008; Kirwan and Megonigal, 2013) makes monitoring the evolution of salt marshes a pressing management imperative as well as a scientific endeavor.

The most closely monitored properties of salt marsh ecosystems are ecological assemblages and elevation, as they are both essential to understand ecogeomorphic processes (Reed and Cahoon, 1992). For instance, elevation determines flooding frequency and therefore influences pioneer vegetation encroachment (Hu et al., 2015), which in turn affects vertical accretion through inorganic sediment capture (Pennings et al., 2005; Mudd et al., 2004, 2010). Individual plants also react to elevation by modifying their root to shoot length ratios, generating feedbacks between organic material build-up and sediment capture (Mudd et al., 2009). The variable intensity of these ecogeomorphic feedbacks enables salt marshes to accrete in response to variations in sea level, thus maintaining their place in the tidal frame (Kirwan and Temmerman, 2009; Crosby et al., 2016).

The objective detection and analysis of vegetation patterns is a mature field, with habitat mapping commonly undertaken through the analysis of spectral properties such as the Normalized Difference of Vegetation Index (NDVI) (Jucke van Beijma, 2015). NDVI mapping is now mature to the extent that it requires only a minimum of ground-truthing to determine the presence and type of vegetation (Hladik and Alber, 2014). This index has been shown to consistently differentiate vegetated areas from tidal flats (Tuxen et al., 2008) and flooded channels from dry land despite the sensitivity of classification algorithms (Belluco et al., 2006; Wang et al., 2007).

Spectral data sources, however, are not sufficient to provide the topographic information necessary to fully understand morphodynamic processes: although Digital Elevation Models (DEMs) have been successfully generated from habitat maps in the Venice lagoon (Silvestri et al., 2003), additional influences on halophyte distribution such as groundwater circulation (Moffett et al., 2010, 2012) can lead to mismatches between topography and habitats (Hladik et al., 2013). These additional influences on habitat distribution prevent the reliable use of spectral data to infer topography. Furthermore, delineating salt marsh platforms exclusively from spectral sources encourages morphological studies to define salt marshes dominantly from an ecological perspective, whereas the physical setting, most notably the elevation within the tidal frame, plays a key role in maintaining ecosystem health (e.g., Morris et al., 2002).

The topographic data necessary to identify marsh platforms already exist: the multiplication of freely available high resolution topographic datasets from lidar or structure from motion (SfM) techniques means that DEMs of horizontal resolutions below 1 m are increasingly common on salt marshes, and offer vertical accuracies below 20 cm even without correcting for

vegetation (Sadro et al., 2007; Wang et al., 2009; Chassereau et al., 2011). At these resolutions, most scarps and channels are detectable on a DEM, and several automated topographic methods already allow the identification of tidal channel networks (Fagherazzi et al., 1999; Liu et al., 2015). However, contrary to spectral datasets, tools designed to accurately delineate the extent of salt marshes through means other than manual digitization are lacking.

In this study, we propose an unsupervised method to topographically differentiate marsh platforms from tidal flats, which we refer to as Topographic Identification of Platforms (TIP). The TIP method aims to reproducibly and accurately delineate marsh platforms using only a DEM as input, while also reducing identification costs and enabling systematic topographic analyses of multiple salt marshes. The processes that form salt marsh platforms can be described by ecological alternate stable states theory (Schroder et al., 2005) and geomorphic bifurcation models (Fagherazzi et al., 2006; Defina et al., 2007). These processes cause salt marshes to develop a distinctive, biologically-mediated topographic structure consisting of several sub-horizontal platforms, separated from tidal flats and from each other by a subvertical scarp and dissected by incising channels (Temmerman et al., 2007; Marani et al., 2007, 2013). The TIP method exploits this characteristic topography, which is clearly visible on high-resolution DEMs and their associated slope rasters, to identify scarps and steep channel banks. As our method uses topographic signatures of marsh platforms, it will reflect the interplay between sedimentation, erosion, and biomass (Fagherazzi et al., 2012) rather than the distribution of specific macrophyte species and should therefore be complementary to, rather than a replacement for, methods that detect plant zonation on marshes. We compare TIP-detected platforms with six manually digitized platforms from English marshes of different horizontal resolutions, demonstrating the potential of this method for quantitative topographic analyses and short- to mid-term monitoring.

2 Methodology

The TIP method automatically detects scarps and platforms of salt marsh systems from a DEM with no manual calibration requirements. Its general process is described in Fig. 1, and includes the possibility of filtering (step 1) and degrading (step 2) the DEM; the effects of both treatments are examined in the discussion. A slope raster is then generated by fitting a polynomial surface to topographic data and taking the derivative of this surface (Hurst et al., 2012; Grieve et al., 2016) (step 3). Steps 4 and 5 are novel algorithms developed in this study to isolate scarps and platforms. The results of the isolation process are compared to manually generated platforms (step 6) to generate a comparison map (step 7).

2.1 Test sites

We test the TIP method on six sites in England, selected for the availability of airborne lidar data in the form of gridded 1 m resolution rasters, provided by the UK Environment Agency (http://environment.data.gov.uk/ds/survey/), and for the diversity of their morphologies and tidal ranges. For each site, marsh platforms were digitized on an unfiltered and non-degraded DEM at a scale of 1: 2,500, using the open-source software QGIS (step 6 in Fig. 1). Source data were flown in 2012 for all sites, unless noted otherwise. The locations of the selected sites are shown in Fig. 2.

Shell Bay, Dorset (S1) is a shallow bay with a spring tidal range of 2.4 m, located in Poole Harbour, a limited entrance bay (*sensu* Allen (2000)) protected from strong waves. The marshes in Shell Bay display jagged outlines, indicative of low wave and tidal current stress (Leonardi and Fagherazzi, 2014). The Stour Estuary marshes (S2) 6 km upstream of the meso-tidal Stour mouth are subject to a spring tidal range of 3.8 m and stronger tidal currents due to their estuarine fringing position (*sensu* Allen (2000)), and therefore display more linear boundaries. The Stiffkey marshes (S3) are back-barrier marshes (Allen, 2000), which experience a 4.7 m spring tidal range and display signs of erosion and accretion. These recent perturbations to the marsh surface provides an interesting challenge for topographic detection of marsh extents. The macro-tidal Medway estuary marshes (S4, spring tidal range of 6.4 m) were chosen due to the presence of numerous channels in the tidal flats. In order to test the ability of our method in regions with extreme tidal ranges, we also analysed two mega-tidal sites: Jenny Brown's Point marshes (S5, spring tidal range of 9.2 m) and the Parrett estuary (S6, spring tidal range of 11.8 m), where sand dunes, different levels inside the tidal flats, saltings and sunken platforms will test the limits of the method's ability to correctly delineate marshes in these environments.

2.2 Preprocessing Topographic Data

The TIP method isolates marsh platforms from a DEM up to their seaward limits by detecting the topographic signature generated by the development of salt marshes. The definition of landward boundaries can vary significantly with context, and may be defined by a vegetation zonation change (Mo et al., 2015), agricultural parcels, or infrastructure (Feagin et al., 2010). Topographic input data is therefore clipped to the landward limit of the platform, at the discretion of the user. In the preparation stage, local slope is calculated from the DEM by fitting a second order polynomial surface (Hurst et al., 2012) with a circular window radius equal to three times the horizontal resolution of the DEM. The DEM may be passed through a Wiener filter (Wiener, 1949; Robinson and Treitel, 1967) to reduce noise from lidar datasets and/or degraded by averaged subsampling before the determination of slope to match complementary datasets. The effect of enabling these optional treatments is further discussed in the results section. Although methods exist to account for vegetation cover in the DEM (Hladik and Alber, 2012; Wang et al., 2009; Sadro et al., 2007; Chassereau et al., 2011; Montané and Torres, 2006), we chose not to apply these corrections as we wanted to ensure that the TIP method can be applied without information on the vegetation assemblages at a given site.

2.3 Scarp routing

Tidal flats and salt marshes occur mostly on low energy coasts (Allen, 2000), characterized by low local relief and slopes. They therefore display similar local slope values, and this parameter alone is insufficient to differentiate between tidal flats and marsh platforms. Likewise, although marsh platforms are locally higher than tidal flats and channels, this may not be the case for extensive marsh systems, where long-shore declivity may cause portions of the tidal flats to be higher than distant emergent platforms. Therefore, elevation alone, though it may be used to visually identify salt marsh platforms, is insufficient for objective platform detection. We address this problem by investigating transition features such as channel banks and erosion scarps, which are outliers in both slope and elevation rasters. These features are commonly defined by steep local slopes,

Earth Surf. Dynam. Discuss., https://doi.org/10.5194/esurf-2017-60
Manuscript under review for journal Earth Surf. Dynam.
Discussion started: 1 November 2017

particularly in mature and eroding systems (Defina et al., 2007; Marani et al., 2013). Furthermore, scarps connect marsh platforms to tidal flats, and therefore represent a distinct break in elevation between the two. However, newly formed or seasonal marshes up to the establishment phase of development (Corenblit et al., 2015) have little impact on local topography and will not have formed platforms: they are unlikely to be detected by a topographic method. In this study, we therefore focus on the identification of scarps and steep channel banks as a precursor to the detection of platforms, referred to as step 4 in Fig. 1.

To reduce computational costs, we delineate an initial search space to initiate the detection of scarps by isolating steep areas of the landscape, weighted by their elevation. We first calculate the relief of each pixel, R_i,

$$R_i = z_i - z_{min}, \tag{1}$$

where z_i [dimensions L] is the elevation of the pixel and z_{min} [L] is the minimum elevation in the DEM. We then divide this relief by the maximum relief in the DEM to get a dimensionless relief at each pixel, R_i^*:

$$R_i^* = \frac{R_i}{z_{max} - z_{min}} \tag{2}$$

A similar procedure is followed for slope, where Rs [dimensionless] is determined by the slope at a pixel, S_i minus the minimum slope S_{min}:

$$Rs_i = S_i - S_{min}, \tag{3}$$

and the dimensionless version is calculated as:

$$Rs_i^* = \frac{Rs_i}{S_{max} - S_{min}} \tag{4}$$

We then multiply these two metrics at each pixel to create the dimensionless parameter P_i^* at each pixel:

$$P_i^* = R_i^* Rs_i^* \tag{5}$$

This dimensionless product is useful for highlighting steep areas at high elevations (Fig. 3): the higher the value of P_i^*, the steeper and higher the pixel is. P_i^* could vary between 0 and 1, where a value of 0 would mean that a pixel was at both the lowest elevation and gradient in the DEM, and vice-versa for a value of 1.

We use the properties of the distribution of P^* to define the first search space, which we call Ss_1. With the exception of macrotidal sites S5 and S6, the pdf of P^* decreases monotonically with increasing P^*, and at sites S5 and S6 the pdf decreases monotonically after a peak value (Fig. 3a). When $f(P^*) < \max(f(P^*))$ and $P^* > \max(P^*)$, the derivative of the pdf is negative and

Earth Surf. Dynam. Discuss., https://doi.org/10.5194/esurf-2017-60
Manuscript under review for journal Earth Surf. Dynam.
Discussion started: 1 November 2017

increasing, i.e., the slope of the pdf curve becomes gentler with increasing P^*. We therefore define the threshold value P^*_{th} where the slope of the pdf is equal to a threshold slope, Sp_{thresh}, on the declining limb of the pdf curve (Fig. 3a). In this study we optimize the threshold value Sp_{thresh} to improve the classification of each site, as described in the Results section. The first search space, Ss_1, is defined as those pixels where $P^* > P^*_{th}$, as shown in Fig. 3b. The search space Ss_1 is also schematically represented as grey cells in Fig. 4a (step 4.1)

We then define a square kernel K_3 of 3 cells in width around each cell in Ss_1. If more than one cell of K_3 is included in Ss_1, the cell containing the local slope maximum in K_3 is flagged as a first order scarp cell Sc_1. If one given K_3 already contains an Sc_1 cell that is not the central cell, the central cell will be flagged as an Sc_1 if and only if it is the next local maximum in K_3. This results in a patchwork of first order scarp cells (step 4.2 in Fig. 4a).

For each first order scarp cell Sc_1, we then flag two second order cells Sc_2 as neighboring cells with the next steepest slopes contained in the search space and not in contact with each other (red outlines in Fig. 4b). If two Sc_1 cells are adjacent, only the cell with the higher slope will be flagged as a Sc_2 cell (step 4.3 in Fig. 4b). This generates a patchwork of first order cells (black outlines Fig. 4b) flanked by one or two second order cells (red outlines in Fig. 4b). Starting from the second order cells Sc_2, we prolong the scarps by finding the cell with the steepest slope that is not adjacent to another identified scarp cell of two lesser orders, within a K_3 kernel centered on the previously identified cell. For example, on the third iteration Sc_3 cells are identified in a K_3 kernel centered on a Sc_2 cell and must not be adjacent to an Sc_1 cell. Generally, Sc_n cells are identified in a K_3 kernel centered on a Sc_{n-1} cell and must not be adjacent to an Sc_{n-2} cell. This routing procedure is applied in all kernels containing no more than two scarp cells and repeated until no cells fit the conditions or the order n is equal to 100 (blue outlines, step 4.4 in Fig. 4b).

This procedure produces a large number of scarps: small creeks within the platform and in higher portions of the tidal flat tend to be selected during this procedure. We use a further algorithm to thin these scarps and eliminate creeks. The first procedure eliminates low elevation scarps. We first define a kernel of 9 cells in width K_9 (i.e., a square kernel of 81 pixels with the pixel being interrogated at its center) and compare its maximum elevation max(ZK_9) to the 75th percentile q_{75} of the entire DEM. Cells that do not satisfy the condition $\max(ZK_9) > ZK_{thresh} \times q_{75}$ are discarded from the finale ensemble of scarps (step 4.5 in Fig. 4c), where ZK_{thresh} is a parameter which we optimize below. Each K_9 kernel containing less than 8 flagged cells is then discarded from the ensemble of scarps; after this procedure finishes we are left with the final ensemble of scarps (step 4.6 in Fig. 4d).

2.4 Platform identification

We identify marsh platforms based on the final ensemble of scarps (step 5 in Fig. 1). The final ensemble of scarps becomes a new search space Ss_2. We then create a square kernel 3 cells in width (K_3) around each cell in this new search space. Using this kernel we identify first order platform cells, Pc_1, which are defined as all cells within K_3 that have higher elevation values than the central cell of the kernel (i.e., those that are higher in elevation than the cells in the final scarp ensemble). We do this because platform cells are located at higher elevations than the scarp cells separating them from tidal flats. We use a kernel rather than a simple blanket elevation threshold over the entire DEM because longitudinal elevation variations may cause some

Earth Surf. Dynam. Discuss., https://doi.org/10.5194/esurf-2017-60
Manuscript under review for journal Earth Surf. Dynam.
Discussion started: 1 November 2017

tidal flat cells to be higher than scarp cells. Each Pc_1 cell that is not adjacent to at least 2 other Pc_1 cells is considered a product of isolated situations and eliminated from the ensemble of platform cells.

Following this initial selection of platform cells, we proceed to iteratively fill the platforms. At this point, the initial ensemble of platform cells, Pc_1, is clustered around the final ensemble of scarps since we have only used a 3 pixel wide kernel centered on scarp cells to create the ensemble of Pc_1 cells. We then iterate using a filling algorithm. The first iteration uses the cells Pc_1, the second Pc_2, and so on. In each iteration of Pc_n cells, new cells are identified using two kernels. First, we define a local elevation condition using an 11 pixel wide kernel K_{11}: we find the maximum elevation in this kernel and then subtract 20 cm to define the minimum local elevation for a platform pixel. The 20 cm leeway is applied to account for local elevation variations on the platforms. We then use a 3 pixel wide kernel K_3 within K_{11} to identify any cells in the next iterations' platform ensemble (Pc_{n+1}). These cell must meet two conditions: i) that they are higher than the local elevation threshold identified with the 11 pixel kernel, and ii) that their distance to the nearest cell in the final scarp ensemble is greater than their distance to platform cells from previous iterations. The first condition is simply to ensure the platform is indeed a low relief surface, and the second is to ensure the iterative process fills the platform away from the scarps. The second condition is also necessary to ensure the platform filling process does not cross scarps. This iterative process is repeated until n reaches an arbitrary value of 100, found to be sufficient to fill the entirety of the platform surface area for our sites.

This process results in platforms surfaces that are spatially continuous, but in some instances sections of the tidal flat with relatively high elevations may also have been identified as marsh platforms. These areas are lower than marsh platforms by the height of the scarp separating them. We filter these cells by using the elevation properties of the entire DEM. A number of authors have shown that there is a gap in the probability distribution of elevations in intertidal landscapes that separates the majority of tidal flats from the majority of marsh platforms in micro-tidal environments (e.g., Fagherazzi et al., 2006; Defina et al., 2007; Carniello et al., 2009). Such a separation, demonstrated by the decrease in probability between the grey and blue surfaces in Fig. 5 is also observed in our meso- and macro-tidal sites, including mega-tidal environments such as the Parrett estuary (Fig. 11). We search for this separation using the probability distribution of elevation, $pdf(z)$ of all cells Pc_n, divided in 100 elevations bins. We determine that the most frequent elevation bin $z_{max(pdf(z))}$ is the most likely to contain cells correctly assigned to the platform ensemble, as the relief of marsh platforms is lower than that of tidal flats. Therefore, only elevations lower than $z_{max(pdf(z))}$ may contain cells misidentified as marsh platforms.

We then must identify which cells from the population of cells lower than $z_{max(pdf(z))}$ form part of the platform, and which do not. To do this, we truncate low elevations that have a low probability (See red curves in Fig. 5). If we did not do this we would have a long tail of low elevations from our initial platform identification. We take the probability distribution of the elevation of the remaining platform cells and calculate the mean probability $\bar{pdf}$ (i.e., we average the probability from the 100 bins). We then search for rz_{thresh} consecutive elevation bins that lie below the elevation of the maximum probability elevation that have lower probabilities than this average. The reason we use consecutive bins is that we do not want the minimum elevation to be determined by a single low probability elevation that has spuriously arisen from the binning process. Once we find rz_{thresh} consecutive elevation bins meeting these criteria we remove all cells lower and including the highest cell that lies within the rz_{thresh} consecutive bins. We optimize the parameter rz_{thresh} below.

Earth Surf. Dynam. Discuss., https://doi.org/10.5194/esurf-2017-60
Manuscript under review for journal Earth Surf. Dynam.
Discussion started: 1 November 2017

Having eliminated these low elevation, low probability cells, we also mark all cells higher than $z_{max(f(z))}$ as platform cells. This may still out leave pools and pansm and platform edges remain jagged. Our final procedure aims to eliminate these artifacts using the following procedure: for a given value of the order *n*, we search in the ensemble of Pc_n cells for cells that are surrounded by more than 6 *Pc* cells of any order within a K_3 kernel. The 2 or less empty cells in K_3 are then attributed the order *n-1*. By iterating through values of *n*, starting with the order 100 and finishing with the order 2, we progressively fill pools and jagged borders of the platform (Fig. 6a). Choosing 6 as the minimal number of platforms cells in each K_3 necessary to execute this "reverse filling" procedure, we ensure that no headlands are generated. We then integrate scarp cells that are connected to platform cells into the platform ensemble with an order greater than 100. We then repeat the "reverse filling" process (Fig. 6b) and execute low-elevation elimination procedure (See blue curves in Fig. 5) to obtain the final platform ensemble.

3 Results and discussion

In order to evaluate the performance of the TIP method, we compare its outputs to manually digitized platforms for all of our test sites (step 7 in Fig. 1). The results are classified as follows: true positives correspond to matching marsh platform cells in the tested (automatically processed) and reference (manually digitized) outputs, true negatives to matching tidal flats, false positives to marsh platforms identified using TIP that are tidal flats in digitized maps, and false negatives where TIP identifies tidal flats in locations that have been digitized as marsh platforms. The performance of the method is then evaluated using three metrics based on the numbers of true positive (*TP*), true negative (*TN*), false positive (*FP*), and false negative (*FN*) cells respectively. The accuracy *Acc* (Fawcett, 2006) describes the likelihood of cells in the tested raster corresponding to the reference raster:

$$Acc = \frac{TP + TN}{TP + TN + FP + FN} \tag{6}$$

We also test the performance of the method by reporting two other metrics: the precision, *Pre*, and the sensitivity, *Sen* (Fawcett, 2006). The precision represents the likelihood of the tested raster overestimating the positives compared to the reference:

$$Pre = \frac{TP}{TP + FP} \tag{7}$$

Conversely, the sensitivity *Sen*, represents the likelihood of the tested raster missing positives compared to the reference:

$$Sen = \frac{TP}{TP + FN} \tag{8}$$

If the results of the TIP method perfectly matched that of the manual digitization, all three metrics would have a value of 1.

Earth Surf. Dynam. Discuss., https://doi.org/10.5194/esurf-2017-60
Manuscript under review for journal Earth Surf. Dynam.
Discussion started: 1 November 2017

3.1 Parameter optimisation

The TIP method contains three user-defined, non-dimensional parameters occurring in sequence during the detection process. The first parameter, Sp_{thresh}, determines the threshold value P^*_{th} for the high-pass filter leading to the selection of the initial search space, shown in Fig. 3a. The parameter Sp_{thresh} influences the solution of the equation $\frac{df}{dP^*} = Sp_{thresh}$. The second parameter, ZK_{thresh} determines the condition on the refinement of existing scarps in the high-pass filter $max(ZK_9) > ZK_{thresh} \times q_{75}$, schematically represented in Fig. 4. The third parameter, rz_{thresh} is used in the platform dispersion process to determine which percentage of the elevation range below $\bar{pdf}$ is maintained in the platform ensemble. In this study, these parameters were set to maximize the average accuracy $\bar{Acc}$ across test sites (Fig. 7): the optimized values (Sp_{thresh}=-2.0, ZK_{thresh}=0.85, rz_{thresh}=8) were used for the subsequent performance analysis. Users may modify these parameters as directed in the code documentation to better fit their study sites.

3.2 Performance analysis

We report the performance of the TIP method for all six sites in Fig. 8, discriminating between the use or absence of a Wiener filter and evaluating the influence of progressive resolution degradation. We find the method's accuracy to be on average of 94.8% at the data's native resolution of 1 m, whether we apply a Wiener filter (Fig. 8a2) or not (Fig. 8a1). This high accuracy signifies that the method can be used to determine the marsh platform extent within 5% of a reference value, as shown in Fig. 9a; this standard is not preserved in perimeter estimates (Fig. 9b). For resolutions of 3 m or less, the accuracy remains on average above 90% when no filter is applied, with however a decrease in accuracy and a departure from the 5% buffer in area correspondence in micro- to meso-tidal sites S1 and S2 when a Wiener filter is applied. We attribute this phenomenon to the more jagged contours of these sites (see Fig. 10a and b), which coarser grids and denoised rasters do not detect. The effect of grid size is also translated in the strong decrease in detected perimeter observed in Fig. 9b; this is because less complex contours lead to shorter boundaries. Such outlines are also more likely to be blurred by the use of a Wiener filter, as demonstrated by the generally lower precision of sites S1 and S2 when using a Wiener filter (Fig. 8b2). This diminution in precision is compensated by higher average sensitivity values when using a Wiener filter (compare Fig. 8c2 to Fig. 8c1). We therefore suggest that all three metrics are used when testing this method on a study site, as no combination of two metrics provides comprehensive insight as to eventual mismatches. Furthermore, although average accuracies remain above 85% for resolutions of 4 to 5 m, we recommend caution when using the method at these resolutions, particularly in micro- to meso-tidal settings where features may be smoothed beyond the method's recognition capacities. Use of the TIP method is not recommended for resolutions coarser than 5m due to the very low accuracies observed for our test sites, making the TIP method adapted to high-resolution data sources such as lidar or photogrammetry.

Figures 10 and 11 show how the morphology of the landscapes influences the performance of the TIP method. Figure 10a shows that in micro-tidal environments, the method tends to overestimate the extent of the marsh platform (seen as false positives), as is confirmed by the higher peak probability of detected platforms as well as the low elevation abrupt tail shown in Fig. 11a. This is the product of two combined factors: (i) identified scarps are not always complete in micro-tidal environmental

where scarps are small and more liable to sub-threshold elimination (see Fig. 4, step 4.5); and (ii) the reverse dispersion process (see Fig. 6) is then likely to encroach on the tidal flat, generating a high number of false positives (see the high left-hand tail in Fig. 11a). This process is different from the generation of false positives in Fig. 10 c-f, although the sharp cut-off at the lowest tail of the elevation distribution in Fig. 11 does not show this difference. In these cases, the position of the scarp line differs between the digitized and the TIP-detected platforms due to elevated portions of the tidal flat being back-to-back with the marsh platform. This suggests that some areas of the tidal flat are topographically closer to the platform than to the rest of the tidal flat and may represent areas likely to be colonized by pioneer vegetation. Conversely, sunken platforms (also called saltings in mega-tidal environments where they may be small and numerous) that are not delineated by scarps may generate false negatives, as seen in the central area of Fig. 10e. Most false negatives are however generated by a stricter elimination of tidal creeks by the TIP method than by manual digitization, a trait particularly visible in Fig. 10b and d. This result confirms that topographic analyses of coastal marshes require a simultaneous analysis of tidal creeks, which can be identified from lidar data using established methods such as those of Fagherazzi et al. (1999) and Liu et al. (2015). Fig. 10c also demonstrates that accreting meander banks may be correctly located in large channels, while sand bars inside these channels are correctly excluded from the platform ensemble. This indicates that the use of creek detection methods, while adding an element to topographic analyses, is unlikely to affect the platform properties.

3.3 Potential for operational monitoring

As well as providing us with the ability to automate the delineation and analysis of marsh platforms across multiple sites, our method also allows the objective detection of change in marsh extent through time, with important implications for habitat monitoring or carbon storage evaluation. We test the capacity of the TIP method to monitor temporal change through the example of site S6, which was affected by heavy rainfall in the summer of 2007. Rivers such as the Parrett carried high discharges, and 1 m lidar data distributed by the Environment Agency shows that between March and October 2007 the North-Eastern corner of site S6 underwent significant erosion. Blue pixels indicating loss of elevation (between March and October) in Fig. 12a bear the characteristic shape of slope failures and intersect the platform outline of March 2007 detected both automatically and manually, indicating that the October platform outline should be further inland.

This retreat of the marsh platform is observed both by the objectively classified (Fig. 12b) and the manually digitized platforms (Fig. 12c). However, whereas the digitization effort focuses on the large bank failures, the TIP method also detects small changes in the DEM at the platform margin (visible in Fig. 12a and b), and may detect them as changes in marsh platform extent. Consequently, despite a close correspondence between TIP-determined marsh outlines and digitized outlines (Fig. 12a) near the bank failures, the digitized volume loss is only 81% of the objectively detected volume loss. Pioneer zones, characterized by shallow slopes and rapid, uneven elevation changes, are also likely to generate small topographic differences between the DEMs.

Earth Surf. Dynam. Discuss., https://doi.org/10.5194/esurf-2017-60
Manuscript under review for journal Earth Surf. Dynam.
Discussion started: 1 November 2017

4 Conclusions

In this study we have presented a novel method which uses the topographic signature of salt marsh platforms to determine their seaward extent on high resolution DEMs. By combining non-dimensional search parameters and empirical calibration, it separates marsh platforms from tidal flats with over 90% accuracy for source data of up to 3 m in grid resolution, a result sufficient to allow quantitative morphology analyses and monitoring, particularly for eroding marshes where scarps are clearly defined. Independence from environmental variables means that our method can be used to complement spectral data for identifying plant types, to better understand feedbacks between sedimentation, deposition and biomass. We tested our method on six sites with a wide range of spring tidal ranges and found that tidal range has no significant impact on the detection accuracy. Furthermore, the presence of algae as well as varying vegetation characteristics, which may require specific calibrations with spectral methods (Morris et al., 2005), do not affect our results. Although we did not test the performance of the TIP method on DEM resolutions finer than 1 m, the option of applying a Wiener filter to reduce DEM noise is available to accommodate DEMs generated from unclassified point clouds, which display higher surface roughness. When combined with creek detection methods such as those proposed by Liu et al. (2015), we expect the performance of the TIP method to improve due to the reduction of false negatives. This would also allow the discrimination of channel evolution within the marsh platform and on the tidal flat, allowing us to simultaneously explore the development of marsh platforms and tidal creeks (D'Alpaos et al., 2007, 2010) in sites with strong tidal forcing.

Furthermore, the unsupervised detection of marsh platforms from their topography alone reduces the computational cost of topographic analysis compared to spectral studies. This promotes the consideration of salt marshes as topographic objects as well as ecological systems, facilitating holistic, data-driven studies on salt marsh eco-geomorphic responses, and testing existing models of eco-geomorphic feedback (e.g. Fagherazzi et al., 2012). It also encourages us to think of the topographic object separately from the ecological system: mismatches in their respective boundaries may therefore be used to investigate accretion processes and pioneer zone growth in continuation with the works of Balke et al. (2014) and Hu et al. (2015). The examination of such processes at smaller scales, such as those obtained with terrestrial lidar stations, may also reveal characteristic accretion patterns (Balke et al., 2012) which topographic methods may objectively detect. Other developments of this method may, in time, enable the detection of the spatial extent of other ecosystems, such as riparian wetlands and mangrove limits.

Code and data availability. Our software is freely available for download on GitHub as part of the Edinburgh Land Surface Dynamics Topographic Tools package at https://github.com/LSDtopotools. The software used in this study is available in this release: https://github.com/LSDtopotools/LSDTopoTools_MarshPlatform/releases/tag/v0.2 (Goodwin et al., 2017).

Author contributions. GCHG designed the method with contributions from other authors. GCHG wrote the code and produced the figures, with support from SMM and FJC in integrating methods with existing channel extraction and topographic processing algorithms. GCHG wrote the paper with contributions from other authors.

Competing interests. The authors declare no competing interests.

Acknowledgements. GCHG was supported by a NERC doctoral training partnership grant (NE/L002558/1). SMM was supported by the Leverhulme Foundation (IAF-2014-009). FJC was supported by NERC grant NE/P012922/1. The authors acknowledge the United Kingdom Environment Agency for the consequent amount of lidar data (point cloud and gridded) made freely available through their website. The authors thank Dr. Dimitri Lague for his insightful comments.

References

Allen, J. R. L.: Morphodynamics of Holocene salt marshes: A review sketch from the Atlantic and Southern North Sea coasts of Europe, Quaternary Science Reviews, 19, 1155–1231, doi:10.1016/S0277-3791(99)00034-7, 2000.

Balke, T., Klaassen, P. C., Garbutt, A., Van der Wal, D., Herman, P. M. J., and Bouma, T. J.: Conditional outcome of ecosystem engineering: A case study on tussocks of the salt marsh pioneer Spartina anglica, Geomorphology, 153-154, 232–238, doi:10.1016/j.geomorph.2012.03.002, 2012.

Balke, T., Herman, P. M. J., and Bouma, T. J.: Critical transitions in disturbance-driven ecosystems: Identifying Windows of Opportunity for recovery, Journal of Ecology, pp. 700–708, doi:10.1111/1365-2745.12241, 2014.

Belluco, E., Camuffo, M., Ferrari, S., Modenese, L., Silvestri, S., Marani, A., and Marani, M.: Mapping salt-marsh vegetation by multispectral and hyperspectral remote sensing, Remote Sensing of Environment, 105, 54–67, doi:10.1016/j.rse.2006.06.006, 2006.

Carniello, L., Defina, A., and D'Alpaos, L.: Morphological evolution of the Venice lagoon: Evidence from the past and trend for the future, Journal of Geophysical Research: Earth Surface, 114, 1–10, doi:10.1029/2008JF001157, 2009.

Chassereau, J. E., Bell, J. M., and Torres, R.: A comparison of GPS and lidar salt marsh DEMs, Earth Surface Processes and Landforms, 36, 1770–1775, doi:10.1002/esp.2199, 2011.

Chmura, G. L., Anisfeld, S. C., Cahoon, D. R., and Lynch, J. C.: Global carbon sequestration in tidal, saline wetland soils, Global Biogeochemical Cycles, 17, 12, doi:1111 10.1029/2002gb001917, 2003.

Corenblit, D., Baas, A., Balke, T., Bouma, T., Fromard, F., Garófano-Gómez, V., González, E., Gurnell, A. M., Hortobágyi, B., Julien, F., Kim, D., Lambs, L., Stallins, J. A., Steiger, J., Tabacchi, E., and Walcker, R.: Engineer pioneer plants respond to and affect geomorphic constraints similarly along water-terrestrial interfaces world-wide, Global Ecology and Biogeography, 24, 1363–1376, doi:10.1111/geb.12373, 2015.

Costanza, R., Arge, R., Groot, R. D., Farberk, S., Grasso, M., Hannon, B., Limburg, K., Naeem, S., O'Neill, R. V., Paruelo, J., Raskin, R. G., Suttonkk, P., and van den Belt, M.: The value of the world ' s ecosystem services and natural capital, Nature, 387, 253–260, doi:10.1038/387253a0, 1997.

Coverdale, T. C., Brisson, C. P., Young, E. W., Yin, S. F., Donnelly, J. P., and Bertness, M. D.: Indirect human impacts reverse centuries of carbon sequestration and salt marsh accretion, PLoS ONE, 9, 1–7, doi:10.1371/journal.pone.0093296, 2014.

Crosby, S. C., Sax, D. F., Palmer, M. E., Booth, H. S., Deegan, L. A., Bertness, M. D., and Leslie, H. M.: Salt marsh persistence is threatened by predicted sea-level rise, Estuarine, Coastal and Shelf Science, 181, 93–99, doi:10.1016/j.ecss.2016.08.018, 2016.

D'Alpaos, A., Lanzoni, S., Marani, M., Bonometto, A., Cecconi, G., and Rinaldo, A.: Spontaneous tidal network formation within a constructed salt marsh: Observations and morphodynamic modelling, Geomorphology, 91, 186–197, doi:10.1016/j.geomorph.2007.04.013, 2007.

D'Alpaos, A., Lanzoni, S., Marani, M., and Rinaldo, A.: On the tidal prism-channel area relations, Journal of Geophysical Research: Earth Surface, 115, 1–13, doi:10.1029/2008JF001243, 2010.

Day, J. W., Britsch, L. D., Hawes, S. R., Shaffer, G. P., Reed, D. J., Cahoon, D., Britsch, L. D., Reed, D. J., Hawes, S. R., and Cahoon, D.: Pattern and process of land loss in the Mississippi Delta: A spatial and temporal analysis of wetland habitat change, Estuaries, 23, 425, doi:10.2307/1353136, 2000.

Defina, A., Carniello, L., Fagherazzi, S., and D'Alpaos, L.: Self-organization of shallow basins in tidal flats and salt marshes, Journal of Geophysical Research: Earth Surface, 112, 1–11, doi:10.1029/2006JF000550, 2007.

Duarte, C. M., Dennison, W. C., Orth, R. J. W., and Carruthers, T. J. B.: The charisma of coastal ecosystems: Addressing the imbalance, Estuaries and Coasts, 31, 233–238, doi:10.1007/s12237-008-9038-7, 2008.

Fagherazzi, S., Bortoluzzi, A., Dietrich, W. E., Adami, A., Lanzoni, S., Marani, M., and Rinaldo, A.: Tidal networks 1. Automatic network extraction and preliminary scaling features from digital terrain maps, Water Resources Research, 35, 3891–3904, doi:10.1029/1999WR900236, 1999.

Fagherazzi, S., Carniello, L., D'Alpaos, L., and Defina, A.: Critical bifurcation of shallow microtidal landforms in tidal flats and salt marshes, Proceedings of the National Academy of Sciences, 103, 8337–8341, doi:10.1073/pnas.0508379103, 2006.

Fagherazzi, S., Kirwan, M. L., Mudd, S. M., Guntenspergen, G. R., Temmerman, S., Rybczyk, J. M., Reyes, E., Craft, C., and Clough, J.: Numerical models of salt marsh evolution: Ecological, geormorphic, and climatic factors, Review of Geophysics, 50, 1–28, doi:10.1029/2011RG000359, 2012.

Fawcett, T.: An introduction to ROC analysis, Pattern Recognition Letters, 27, 861–874, doi:10.1016/j.patrec.2005.10.010, 2006.

Feagin, R. A., Martinez, M. L., Mendoza-Gonzalez, G., and Costanza, R.: Salt marsh zonal migration and ecosystem service change in response to global sea level rise: A case study from an urban region, Ecology & Society, 15, 1–15, http://www.ecologyandsociety.org/vol15/iss4/art14/, 2010.

Goodwin, G. C. H., Mudd, S. M., and Clubb, F. J.: LSDtopotools Marsh Platform Identification Tool, Tech. rep., Zenodo, doi:10.5281/zenodo.1007788, 2017.

Grieve, S. W. D., Mudd, S. M., Milodowski, D. T., Clubb, F. J., and Furbish, D. J.: How does grid-resolution modulate the topographic expression of geomorphic processes?, Earth Surface Dynamics, 4, 627–653, doi:10.5194/esurf-4-627-2016, 2016.

Hladik, C. and Alber, M.: Accuracy assessment and correction of a LIDAR-derived salt marsh digital elevation model, Remote Sensing of Environment, 121, 224–235, doi:10.1016/j.rse.2012.01.018, 2012.

Hladik, C. and Alber, M.: Classification of salt marsh vegetation using edaphic and remote sensing-derived variables, Estuarine, Coastal and Shelf Science, 141, 47–57, doi:10.1016/j.ecss.2014.01.011, 2014.

Hladik, C., Schalles, J., and Alber, M.: Salt marsh elevation and habitat mapping using hyperspectral and LIDAR data, Remote Sensing of Environment, 139, 318–330, doi:10.1016/j.rse.2013.08.003, 2013.

Hu, Z., Van Belzen, J., Van Der Wal, D., Balke, T., Wang, Z. B., Stive, M., and Bouma, T. J.: Windows of opportunity for salt marsh vegetation establishment on bare tidal flats: The importance of temporal and spatial variability in hydrodynamic forcing, Journal of Geophysical Research G: Biogeosciences, 120, 1450–1469, doi:10.1002/2014JG002870, 2015.

Hurst, M. D., Mudd, S. M., Walcott, R., Attal, M., and Yoo, K.: Using hilltop curvature to derive the spatial distribution of erosion rates, Journal of Geophysical Research: Earth Surface, 117, 1–19, doi:10.1029/2011JF002057, 2012.

Jucke van Beijma, S.: Remote Sensing - Based Mapping and Modelling of Coastal Salt Marsh Habitats Based on Optical , Lidar and Sar Data. Thesis submitted for the degree of Doctor of Philosophy at the University of Leicester, Ph.D. thesis, 2015.

Kirwan, M. and Temmerman, S.: Coastal marsh response to historical and future sea-level acceleration, Quaternary Science Reviews, 28, 1801–1808, doi:10.1016/j.quascirev.2009.02.022, http://dx.doi.org/10.1016/j.quascirev.2009.02.022, 2009.

Kirwan, M. L. and Megonigal, J. P.: Tidal wetland stability in the face of human impacts and sea-level rise., Nature, 504, 53–60, doi:10.1038/nature12856, 2013.

Kirwan, M. L., Murray, A. B., Donnelly, J. P., and Corbett, D. R.: Rapid wetland expansion during European settlement and its implication for marsh survival under modern sediment delivery rates, Geology, 39, 507–510, doi:10.1130/G31789.1, 2011.

Leonardi, N. and Fagherazzi, S.: How waves shape salt marshes, Geology, 42, 887–890, doi:10.1130/G35751.1, 2014.

Liu, Y., Zhou, M., Zhao, S., Zhan, W., Yang, K., and Li, M.: Automated extraction of tidal creeks from airborne laser altimetry data, Journal of Hydrology, 527, 1006–1020, doi:10.1016/j.jhydrol.2015.05.058, 2015.

Marani, M., D'Alpaos, A., Lanzoni, S., Carniello, L., and Rinaldo, A.: Biologically-controlled multiple equilibria of tidal landforms and the fate of the Venice lagoon, Geophysical Research Letters, 34, 1–5, doi:10.1029/2007GL030178, 2007.

Marani, M., Da Lio, C., and D'Alpaos, A.: Vegetation engineers marsh morphology through multiple competing stable states., Proceedings of the National Academy of Sciences of the United States of America, 110, 3259–63, doi:10.1073/pnas.1218327110, 2013.

Mo, Y., Momen, B., and Kearney, M. S.: Quantifying moderate resolution remote sensing phenology of Louisiana coastal marshes, Ecological Modelling, 312, 191–199, doi:http://dx.doi.org/10.1016/j.ecolmodel.2015.05.022, 2015.

Moffett, K. B., Robinson, D. A., and Gorelick, S. M.: Relationship of Salt Marsh Vegetation Zonation to Spatial Patterns in Soil Moisture, Salinity, and Topography, Ecosystems, 13, 1287–1302, doi:10.1007/s10021-010-9385-7, 2010.

Moffett, K. B., Gorelick, S. M., McLaren, R. G., and Sudicky, E. A.: Salt marsh ecohydrological zonation due to heterogeneous vegetation-groundwater-surface water interactions, Water Resources Research, 48, doi:10.1029/2011WR010874, 2012.

Möller, I. and Spencer, T.: Wave dissipation over macro-tidal saltmarshes: Effects of marsh edge typology and vegetation change, Journal of Coastal Research, 36, 506–521, doi:ISSN:0749-0208, 2002.

Montané, J. M. and Torres, R.: Accuracy Assessment of Lidar Saltmarsh Topographic Data Using RTK GPS, Photogrammetric Engineering & Remote Sensing, pp. 961–967, doi:0099-1112/06/7208–0961, 2006.

Morris, J. T., Sundareshwar, P. V., Nietch, C. T., Kjerfve, B., and Cahoon, D. R.: Responses of Coastal Wetlands to Rising Sea Level, Ecology, 83, 2869–2877, doi:10.1890/0012-9658(2002)083[2869:ROCWTR]2.0.CO;2, 2002.

Morris, J. T., Porter, D., Neet, M., Noble, P. a., Schmidt, L., Lapine, L. a., and Jensen, J. R.: Integrating LIDAR elevation data, multi-spectral imagery and neural network modelling for marsh characterization, International Journal of Remote Sensing, 26, 5221–5234, doi:10.1080/01431160500219018, 2005.

Mudd, S. M., Fagherazzi, S., Morris, J. T., and Furbish, D. J.: Flow, sedimentation, and biomass production on a vegetated salt marsh in South Carolina: toward a predictive model of marsh morphologic and ecologic evolution, American Geophysical Union, pp. 165–187, doi:10.1029/CE059p0165, 2004.

Mudd, S. M., Howell, S. M., and Morris, J. T.: Impact of dynamic feedbacks between sedimentation, sea-level rise, and biomass production on near-surface marsh stratigraphy and carbon accumulation, Estuarine, Coastal and Shelf Science, 82, 377–389, doi:10.1016/j.ecss.2009.01.028, 2009.

Mudd, S. M., D'Alpaos, A., and Morris, J. T.: How does vegetation affect sedimentation on tidal marshes? Investigating particle capture and hydrodynamic controls on biologically mediated sedimentation, Journal of Geophysical Research: Earth Surface, 115, doi:10.1029/2009JF001566, 2010.

Nardin, W. and Edmonds, D. A.: Optimum vegetation height and density for inorganic sedimentation in deltaic marshes, Nature Geoscience, 7, 722–726, doi:10.1038/ngeo2233, 2014.

Nelson, J. L. and Zavaleta, E. S.: Salt marsh as a coastal filter for the oceans: Changes in function with experimental increases in Nitrogen loading and sea-level rise, PLoS ONE, 7, doi:10.1371/journal.pone.0038558, 2012.

Pennings, S. C., Grant, M. B., and Bertness, M. D.: Plant zonation in low-latitude salt marshes: Disentangling the roles of flooding, salinity and competition, Journal of Ecology, 93, 159–167, doi:10.1111/j.1365-2745.2004.00959.x, 2005.

Reed, D. and Cahoon, D.: The relationship between marsh surface topography, hydroperiod, and growth of Spartina alterniflora in a deteriorating Louisiana salt marsh, Journal of Coastal Research, 8, 77–87, www.jstor.org/stable/4297954, 1992.

Robinson, E. A. and Treitel, S.: Principles of Digital Wiener Filtering, Geophysical Prospecting, 15, 311–332, doi:10.1111/j.1365-2478.1967.tb01793.x, 1967.

Sadro, S., Gastil-Buhl, M., and Melack, J.: Characterizing patterns of plant distribution in a southern California salt marsh using remotely sensed topographic and hyperspectral data and local tidal fluctuations, Remote Sensing of Environment, 110, 226–239, doi:10.1016/j.rse.2007.02.024, 2007.

Schroder, A., Persson, L., de Roos, A. M., and Lundbery, P.: Direct Experimental Evidence for Alternative Stable States: A Review, Oikos, 110, 3–19, doi:10.1111/j.0030-1299.2005.13962.x, 2005.

Shepard, C. C., Crain, C. M., and Beck, M. W.: The protective role of coastal marshes: A systematic review and meta-analysis, PLoS ONE, 6, doi:10.1371/journal.pone.0027374, 2011.

Silvestri, S., Marani, M., and Marani, A.: Hyperspectral remote sening of salt marsh vegetation, morphology and soil topography, Physics and Chemistry of the Earth, 28, 15–25, doi:10.1016/S1474-7065(03)00004-4, 2003.

Temmerman, S., Bouma, T. J., Van de Koppel, J., Van der Wal, D., De Vries, M. B., and Herman, P. M. J.: Vegetation causes channel erosion in a tidal landscape, Geology, 35, 631–634, doi:10.1130/G23502A.1, 2007.

Tuxen, K. A., Schile, L. M., Kelly, M., and Siegel, S. W.: Vegetation colonization in a restoring tidal marsh: A remote sensing approach, Restoration Ecology, 16, 313–323, doi:10.1111/j.1526-100X.2007.00313.x, 2008.

Wang, C., Menenti, M., Stoll, M. P., Belluco, E., and Marani, M.: Mapping mixed vegetation communities in salt marshes using airborne spectral data, Remote Sensing of Environment, 107, 559–570, doi:10.1016/j.rse.2006.10.007, 2007.

Wang, C., Menenti, M., Stoll, M. P., Feola, A., Belluco, E., and Marani, M.: Separation of ground and low vegetation signatures in LiDAR measurements of salt-marsh environments, IEEE Transactions on Geoscience and Remote Sensing, 47, 2014–2023, doi:10.1109/TGRS.2008.2010490, 2009.

Wiener, N.: Extrapolation, interpolation, and smoothing of stationary time series: with engineering applications, Technology Press of the Massachusetts Institute of Technology, 1949.

Earth Surf. Dynam. Discuss., https://doi.org/10.5194/esurf-2017-60
Manuscript under review for journal Earth Surf. Dynam.
Discussion started: 1 November 2017

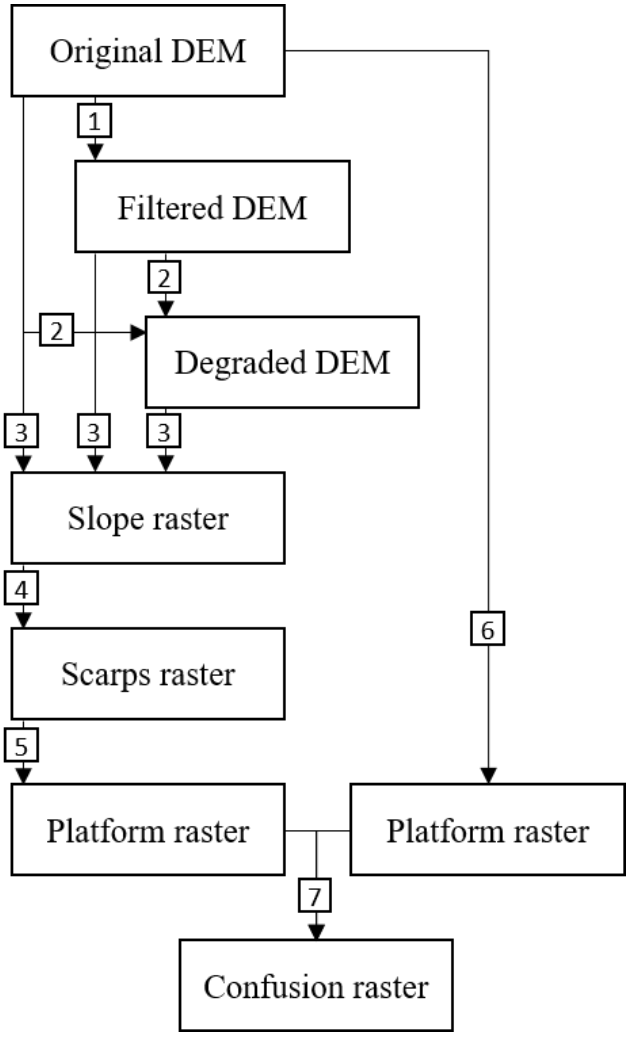

Figure 1. Flow chart showing the overall structure of the TIP method and its validation. Each object (rectangle) is obtained by implementing a routine (square), numbered as follows: 1. Implementation of a Wiener filter (optional); 2. Subsampling by average value (optional); 3. Calculation of slope by fitting a second order polynomial surface; 4. Scarp identification by routing; 5. Platform identification by dispersion; 6. Manual digitization of a marsh platform; 7. Comparison of the objectively detected platform to the manually digitized platform.

Earth Surf. Dynam. Discuss., https://doi.org/10.5194/esurf-2017-60
Manuscript under review for journal Earth Surf. Dynam.
Discussion started: 1 November 2017

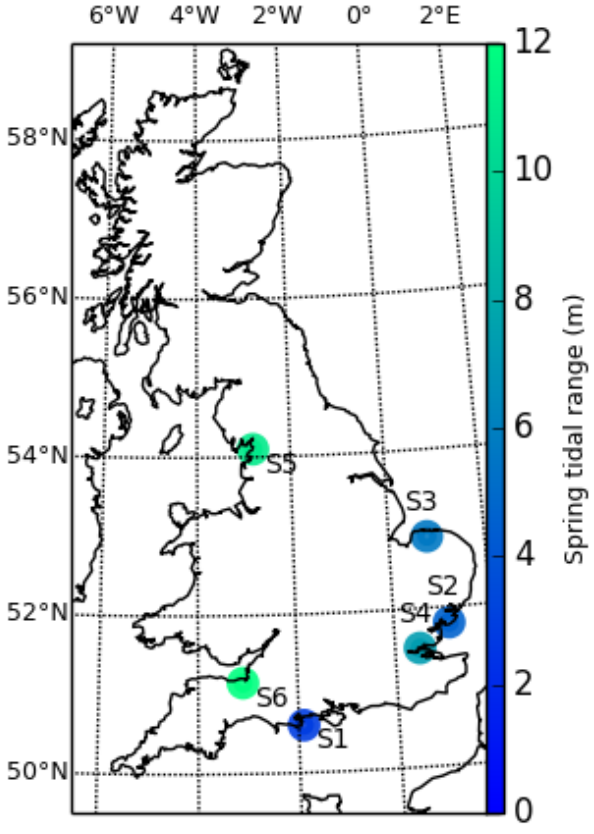

Figure 2. This map shows the six sites selected from the lidar collection of the UK environment agency, colored by spring tidal range. The sites are numbered as follows: S1: Shell Bay, Dorset; S2: Stour Estuary, Suffolk; S3: Stiffkey, Norfolk; S4: Medway Estuary,Kent; S5: Jenny Brown's Point, Lancashire; S6: Parrett Estuary, Somerset.

Earth Surf. Dynam. Discuss., https://doi.org/10.5194/esurf-2017-60
Manuscript under review for journal Earth Surf. Dynam.
Discussion started: 1 November 2017

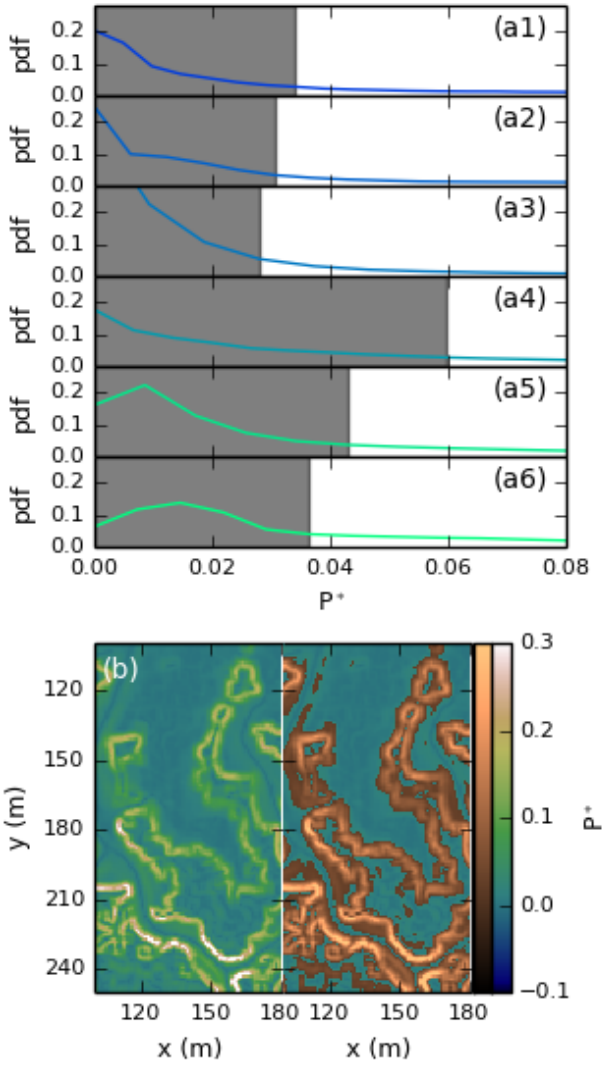

Figure 3. a1-6. Frequency distribution of P^* for sites S1-6. The greyed portion of the plot represents pixels that are not included in the search space Ss_1; b. raster representation of P^* for site S1: Shell Bay. Values of P^* under P^*_{th} use the topographic color scheme, while values above P^*_{th} use the copper color scheme and are included in Ss_1.

Earth Surf. Dynam. Discuss., https://doi.org/10.5194/esurf-2017-60
Manuscript under review for journal Earth Surf. Dynam.
Discussion started: 1 November 2017

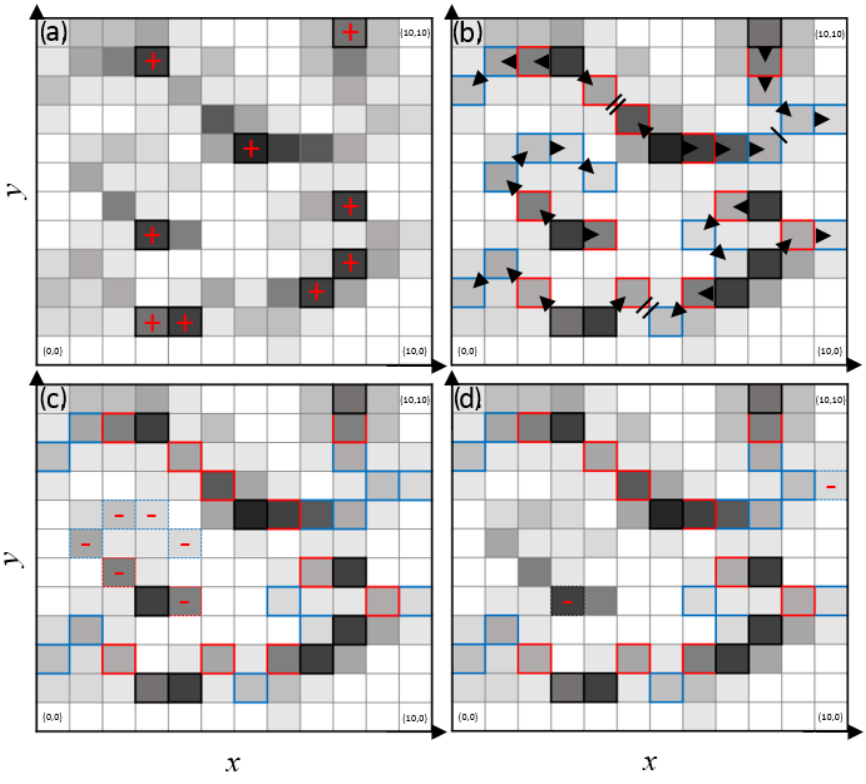

Figure 4. Schematic example of the scarp detection process through maximum slope routing. Panel a. shows two steps. Step 4.1: determination of the search space Ss_1 (greyed cells, darker with arbitrary slope). Step 4.2: Determination of local maxima Sc_1 (black outlines with a plus sign); b. Step 4.3: Determination of Sc_2 cells (red outlines). Step 4.4: Determination of Sc_n cells, n>2 (blue outlines); c. Step 4.5: Elimination of cells where $max(Zk_9) < 0.85 \times q_{75}$ (dashed outlines with a minus sign); d. Step 4.6: Elimination of isolated cells (dashed outlines with a minus sign). The arrows represent the progressive selection of scarp cells.

Earth Surf. Dynam. Discuss., https://doi.org/10.5194/esurf-2017-60
Manuscript under review for journal Earth Surf. Dynam.
Discussion started: 1 November 2017

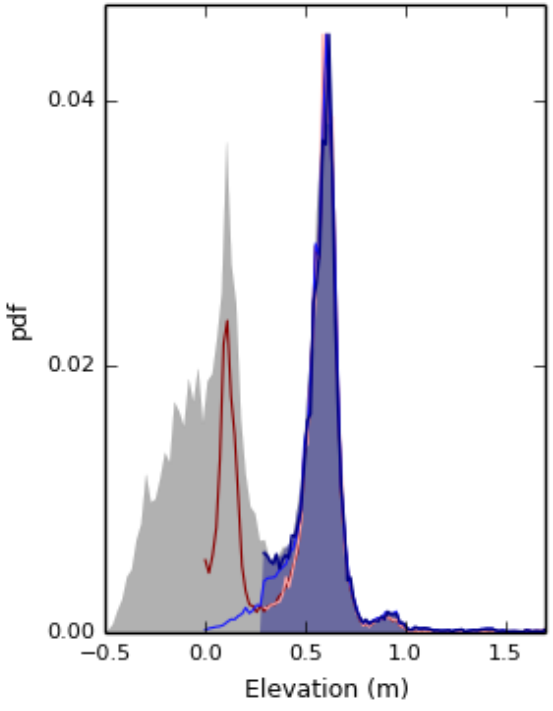

Figure 5. Diagram describing the elimination of the tail of the elevation probability distribution function for site S1. The grey filled surface is the pdf of elevation for the original DEM. The dark red line is the pdf of elevation of the platform after the dispersion process. The orange line is the pdf of elevation of the platform after truncation of the tail of the distribution. The blue line is the pdf of elevation of the platform after filling pools and jagged outlines and after the addition of scarps in the platform ensemble. The dark blue line, associated to the blue filled surface, is the pdf of elevation for the final platform, after the tail of its distribution is truncated a second time. All distributions in this plot were forced to display the same maximum for clarity.

Earth Surf. Dynam. Discuss., https://doi.org/10.5194/esurf-2017-60
Manuscript under review for journal Earth Surf. Dynam.
Discussion started: 1 November 2017

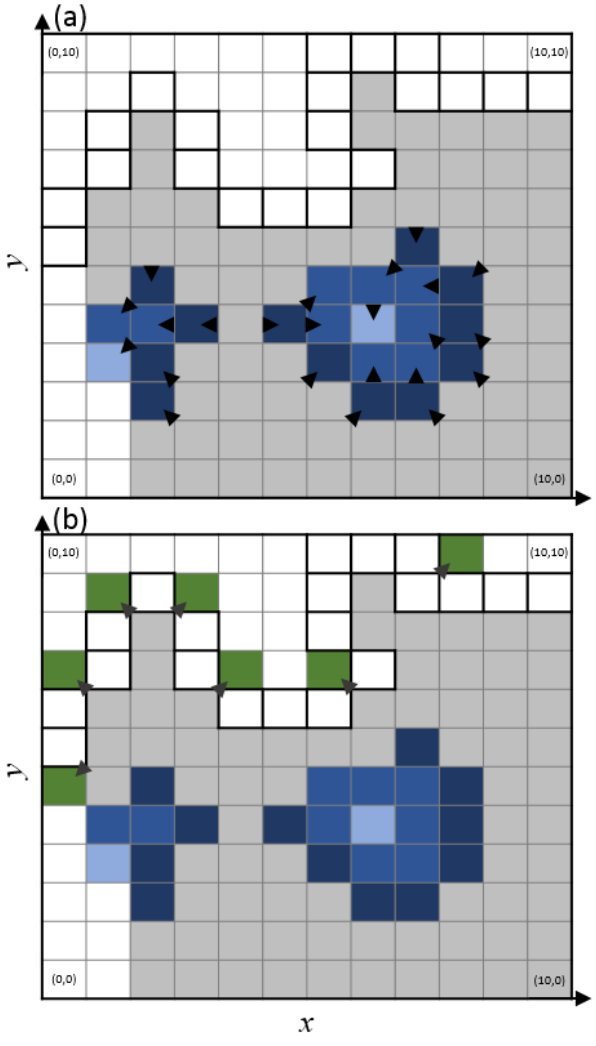

Figure 6. Schematic example of the reverse platform filling process. a. Step 5.1: Filling of empty cells adjacent to Pc_n cells (grey, dark blue and blue cells) with and order *n-1* (dark blue, blue and light blue cells); b. Step 5.2: Filling of empty cells adjacent to Pc_n cells (grey cells) with and order *n-1* (green cells) when scarp cells (black outlines) are included in the platform ensemble. The arrows indicate the dispersion pattern.

Earth Surf. Dynam. Discuss., https://doi.org/10.5194/esurf-2017-60
Manuscript under review for journal Earth Surf. Dynam.
Discussion started: 1 November 2017

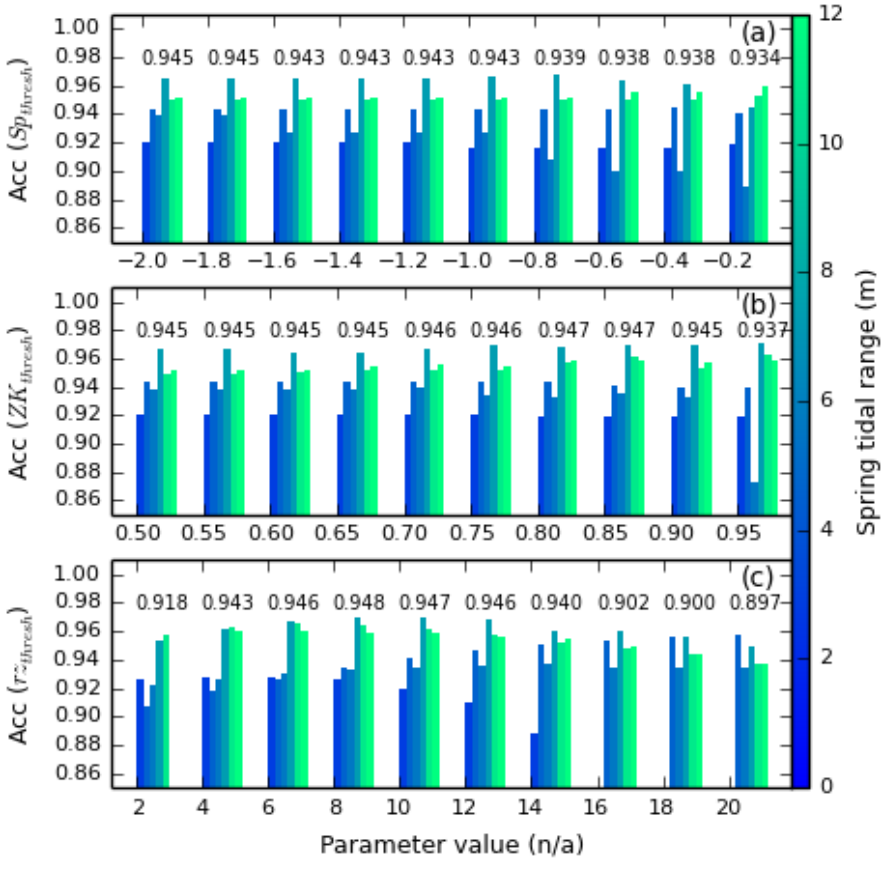

Figure 7. Accuracy charts used to optimize the three user-defined parameters for the six test sites, each site being colored by spring tidal range, with no filter. Each group of bars represents the accuracy for one parameter value when applied to all the test sites. The mean accuracy appears above each group; a. Accuracy for the parameter Opt1. The retained value for Opt1 is -2.0; b. Accuracy for the parameter Opt2. The retained value for Opt2 is 0.85; c. Accuracy for the parameter Opt3. The retained value for Opt3 is 8.

Earth Surf. Dynam. Discuss., https://doi.org/10.5194/esurf-2017-60
Manuscript under review for journal Earth Surf. Dynam.
Discussion started: 1 November 2017

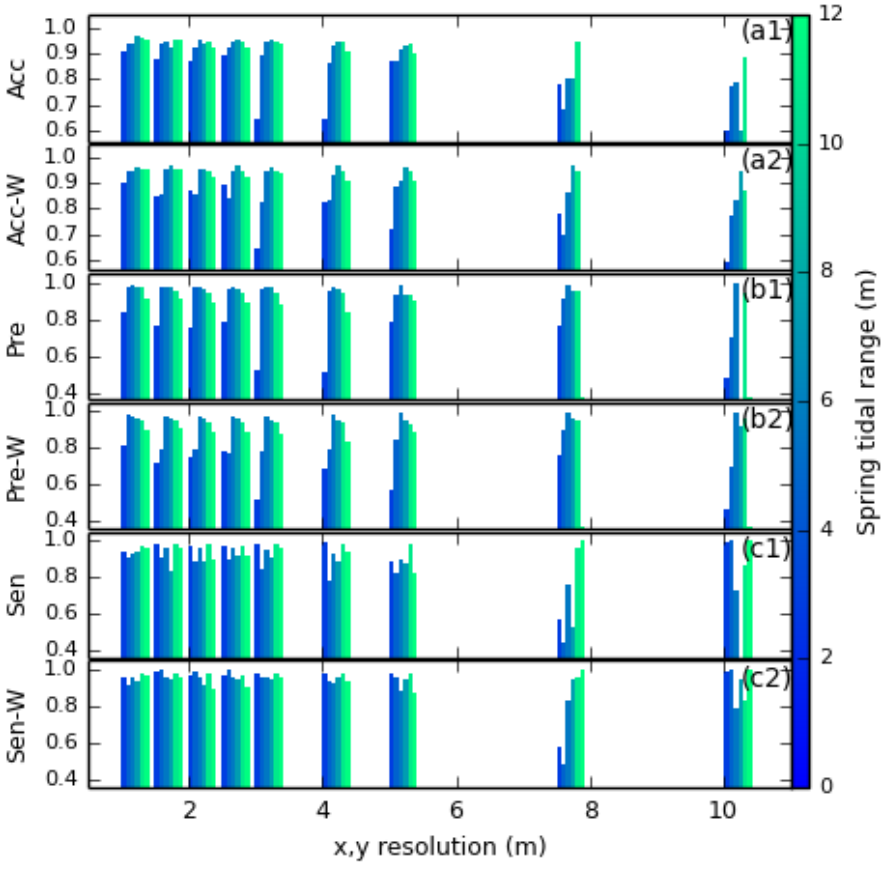

Figure 8. Performance of the platform detection method for all sites, colored according to their spring tidal range; a1. Accuracy of the method when no filter is used; a2. Accuracy of the method when using a Wiener filter; b1. Precision of the method when no filter is used; b2. Precision of the method when using a Wiener filter; c1. Sensitivity of the method when no filter is used; c2. Sensitivity of the method when using a Wiener filter.

Earth Surf. Dynam. Discuss., https://doi.org/10.5194/esurf-2017-60
Manuscript under review for journal Earth Surf. Dynam.
Discussion started: 1 November 2017

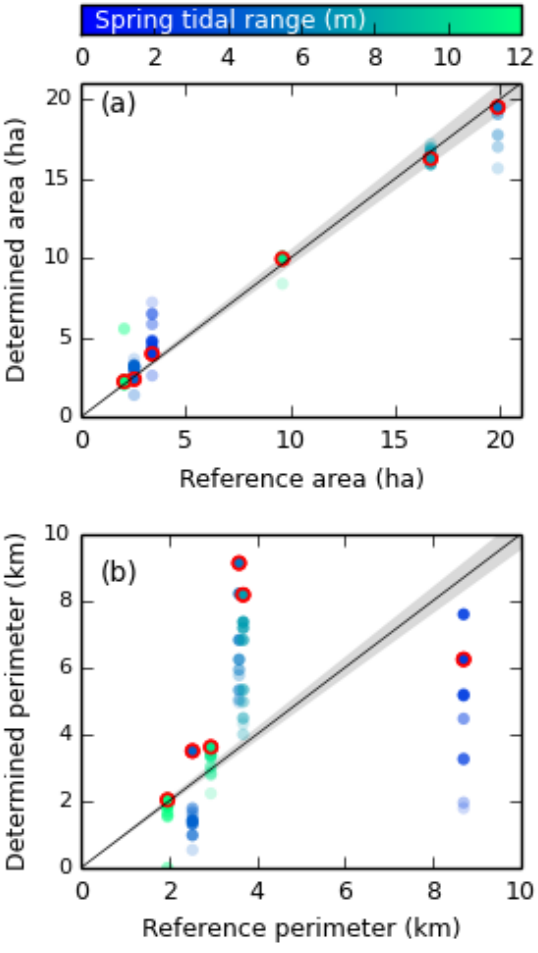

Figure 9. Total area (a) and perimeter (b) of the marsh platform in the reference rasters against the same data in the automatically processed rasters. Data points are colored according to their spring tidal range, with transparency increasing with horizontal resolution. Points circled in red correspond to rasters in their native resolution when using a Wiener filter.

Earth Surf. Dynam. Discuss., https://doi.org/10.5194/esurf-2017-60
Manuscript under review for journal Earth Surf. Dynam.
Discussion started: 1 November 2017

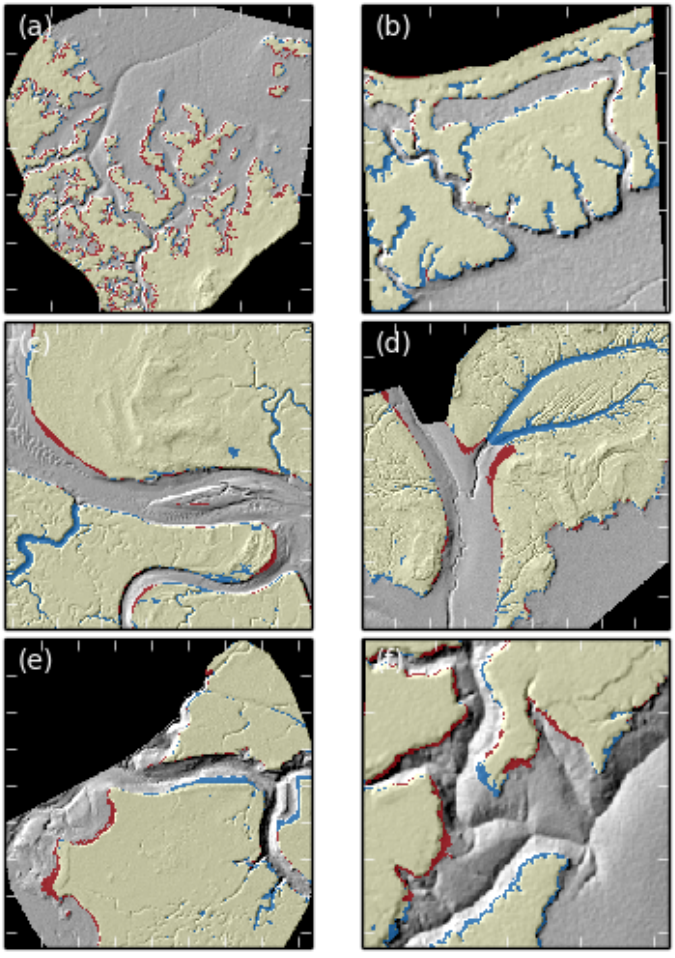

Figure 10. Rasters comparing digitized versus extracted marsh platforms superimposed on hillshade data for all six sites after detection with no Wiener filtering. Black areas are outside of the detection domain and contain no data. Yellow areas correspond to True Positives (TP) and transparent areas to True Negatives (TN). Red areas correspond to False Positives (FP) and blue areas to False Negatives (FN). Ticks are placed 50m apart. The sites are numbered as follows: a: Shell Bay, Dorset; b: Stour Estuary, Suffolk; c: Stiffkey, Norfolk; d: Medway Estuary,Kent; e: Jenny Brown's Point, Lancashire; f: Parrett Estuary, Somerset.

Earth Surf. Dynam. Discuss., https://doi.org/10.5194/esurf-2017-60
Manuscript under review for journal Earth Surf. Dynam.
Discussion started: 1 November 2017

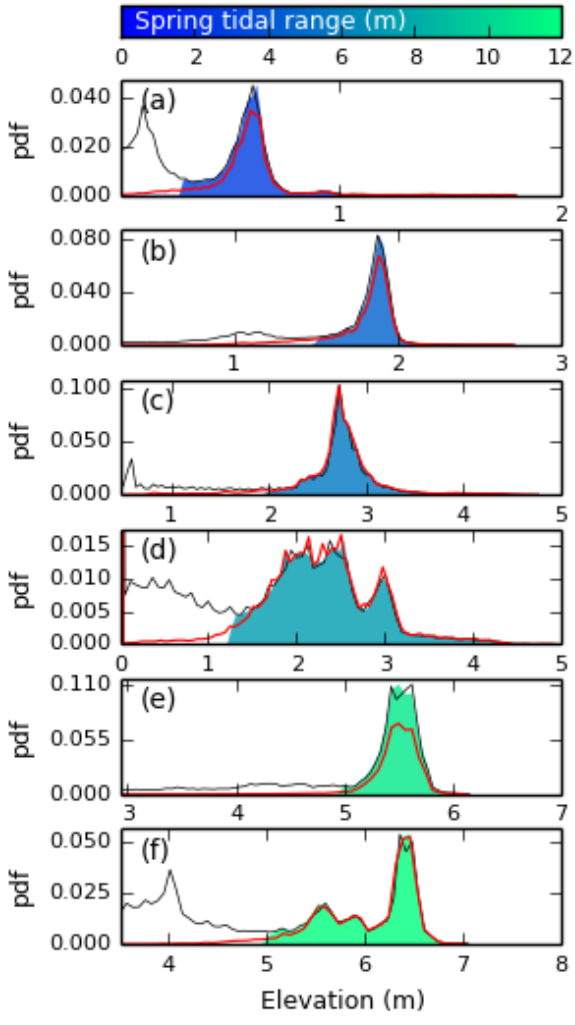

Figure 11. Elevation distribution functions for sites S1 to S6 (plots a. to f. respectively). The red line corresponds to the elevation distribution for the reference rasters. The filled area corresponds to the elevation distribution of the automatically processed rasters, colored according to their spring tidal range. The grey line represents the elevation distribution of the original DEM, with frequency maxima set to match those of the automatically processed rasters so as to nullify the effect of empty cells.

Earth Surf. Dynam. Discuss., https://doi.org/10.5194/esurf-2017-60
Manuscript under review for journal Earth Surf. Dynam.
Discussion started: 1 November 2017

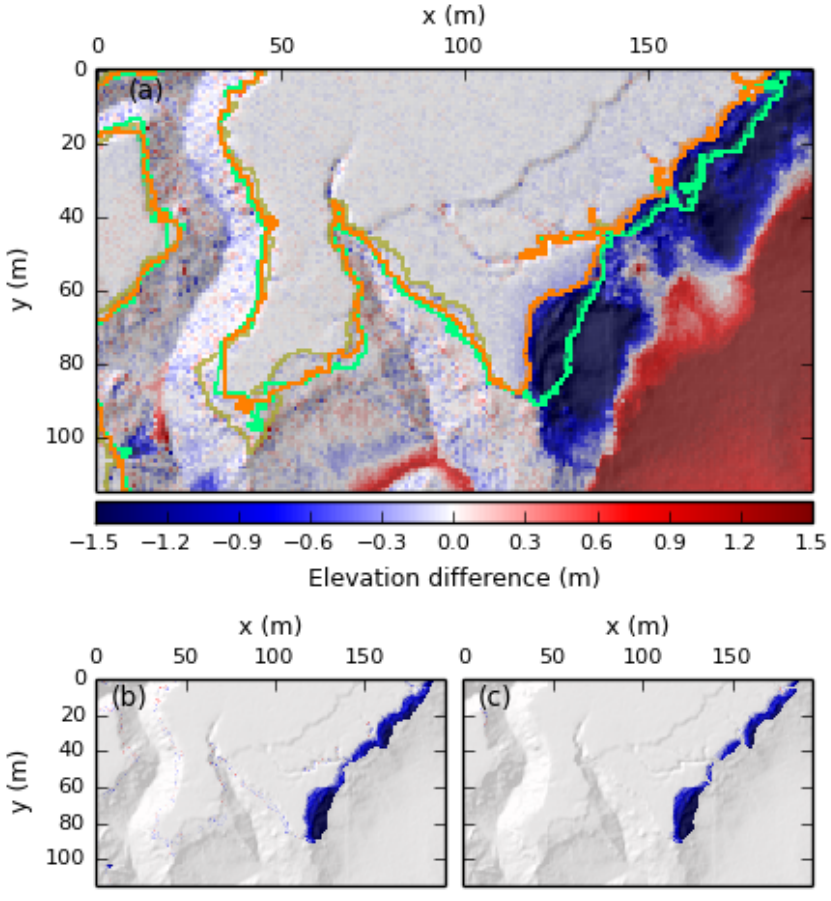

Figure 12. a. Comparison of marsh areas for a portion of S6 between March (green lines) and October (orange lines) 2007, surperimposed on hillshade data of October 2007. Bright lines correspond to the automatically detected marsh boundary, whereas faded lines correspond to digitized marsh boundaries. Colored surfaces indicate elevation gain or loss between March and October 2007; b. Map of elevation loss and gain associated to marsh platform evolution, according to the TIP method. Total volume loss is 1188 m^3; c. Map of elevation loss and gain associated to marsh platform evolution, according to manual digitization. Total volume loss is 966 m^3.